On the development of high order realizable schemes for the Eulerian simulation of disperse phase flows: a convex-state preserving Discontinuous Galerkin method

Macole Sabat[1,2], **Adam Larat**[1,2,4], **Aymeric Vié**[3], **Marc Massot**[*1,2,4]

[1] CNRS, UPR 288, Laboratoire d'Energétique moléculaire et macroscopique, combustion, Grande Voie des Vignes, 92295 Chatenay-Malabry, France
[2] Ecole Centrale Paris, Grande Voie des Vignes, 92295 Chatenay-Malabry, France
[3] Center for Turbulence Research (CTR), Stanford University, Stanford, CA 94305-3024
[4] Fédération de Mathématiques de l'Ecole Centrale Paris, FR CNRS 3487, France

[Received date; Accepted date] - to be inserted later

Abstract

In the present work, a high order realizable scheme for the Eulerian simulation of disperse phase flows on unstructured grids is developed and tested. In the Eulerian modeling framework two approaches are studied: the monokinetic (MK) [1] and the Gaussian closures [2, 3]. The former leads to a pressureless gas dynamics system (PGD). It accurately reproduces the physics of such flows at low Stokes number, but is challenging for numerics since the resulting system is weakly hyperbolic. The latter deals with higher Stokes numbers by accounting for particle trajectory crossings (PTC) [4]. Compared to the MK closure, the resulting system of equation is hyperbolic but has a more complex structure; realizability conditions are satisfied at the continuous level, which imply a precise framework for numerical methods. To achieve the goals of accuracy, robustness and realizability, the Discontinuous Galerkin method (DG) is a promising numerical approach [5, 6, 7, 8]. Based on the recent work of Zhang et al. [6], the DG method used is associated to a convex projection strategy, which respects the realizability constraints without affecting the accuracy. The main contribution of this work is to apply one of the latest developments in the field of numerical methods (DG) to physical models, taking into account the free transport and drag terms of the disperse phase flow, which are the building blocks for the Eulerian modeling based on moments methods. DG results are eventually compared qualitatively and quantitatively to the Lagrangian results and to the reference simulations provided by a second order structured MUSCL/HLL finite volume scheme [9, 3]. Through these comparisons, the DG method is shown to be competitive for the description of such flows.

1. INTRODUCTION

The study of two-phase flows is of considerable importance in many fields of science and technology. In the present contribution we focus on two multiphase regimes, namely droplets flows (discrete fluid droplets in a continuous gas) and particle laden-flows (discrete solid particles in a continuous fluid). These regimes take place in a wide range of applications such as fluidized beds, spray dynamics, atomization of fuel in combustion chamber (multiphase combustion), alumina particles in rocket engines, cosmology, etc.

The simulation of the discrete phase can be done through full direct numerical simulation, which provides a model for the dynamics of the interface between the disperse phase and the continuous phase, as well as the exchanges between these two phases (for more information on the dynamic of interface one can refer to the work of le Chenadec and Pitsch [10] and the references therein). This full resolution at the microscopic level is very rich in information for each droplet and is therefore computationally very expensive. An alternative method, with a coarser level of description and a higher level of modeling and related assumptions can be used for the resolution at the mesoscopic

*corresponding author: marc.massot@ecp.fr

level; it is also called the kinetic approach. It provides a statistical description of the droplets as a cloud of point particles. In this context, the exchanges of mass, momentum and heat are described from a statistical point of view, when the interface behavior and the detailed microscopic properties are not predicted. The number density function (NDF), which is a representation of the particle distribution, satisfies the generalized population balance equation (GPBE) also called the Williams-Boltzmann equation (WBE) in the context of sprays [11]. The internal variables characterizing one particle are for example size, velocity, and temperature, so that the total resulting phase space is high dimensional.

The most accurate and widely used way for solving the GPBE is the Lagrangian-Monte-Carlo method (LMC) [12, 13], especially in the direct numerical simulation (DNS) field. It approximates the NDF by a sample of discrete numerical parcels of particles each of them being solved through a Lagrangian system of ordinary differential equations (ODE). The accuracy of this method is highly linked to the number of parcels. For now, even if LCM is used for DNS, it is still unaffordable for real applications where statistical convergence is required. For more details on the Lagrangian-Eulerian methods one may refer to the literature [14, 15, 16] and references therein. Another way to solve this equation is the macroscopic Eulerian method, which solves for a finite set of integrated quantities over the phase space, called **moments**. The main advantages of the Eulerian approach over the LMC are its ease of coupling with the continuous phase [17] and its inherent statistical convergence, the reasons which promote its usage for high performance computing (HPC) and parallel computing. The loss of information resulting from the use of a finite set of moments can be corrected by applying a suitable closure, which highlights the importance of such a choice [18, 19, 20]. Two main types of moments methods are found in the literature: the algebraic-closure-based moment method (ACBMM) and the kinetic-based moment method (KBMM). The ACBMM is based on algebraic closure founded on physical arguments [21, 18, 19]. The KBMM, on the other hand, is based on the choice of a presumed shape for the NDF having as many parameters as the number of moments one needs to control [1, 22, 4, 23, 24]. The KBMM is used in this work for its advantages in terms of realizability and numerical scheme design. For a comparison between the two appoaches one may refer to the work of Vié et al. [3].

In the present work, we consider the case of high Knudsen number where the particle-particle collisions are negligible. Moreover, since one of the most delicate steps in the Eulerian modeling is the velocity closure for the convective part, we will therefore focus on the transport and drag terms in the WBE. It is essential to note that these terms are the building blocks for all the Eulerian modeling using the moment approach. According to the closure used for the approach and the set of moments taken into account, one can find a hierarchy of Eulerian models. In this context, two models are used. The first model studied in this work is the monokinetic closure model (MK), for which the velocity distribution is a Dirac δ-function [1]. This model correctly reproduces the formation of depletion zones and stiff accumulations regions, which usually occur in the case of low inertia particles (low Stokes numbers). However, for moderate to high Stokes numbers, the occurrence of particle trajectory crossings (PTC) cannot be reproduced by MK. Actually, the PTC lead to a state of multi-velocity which can not be captured by the single Dirac δ-function used for the velocity distribution in the MK closure. The second chosen closure should then account for the coexistence of several velocities at the same location in order to correctly reproduce the PTC. Among the full hierarchy of closures, the Gaussian closure is considered hereafter [2, 3], which is the simplest model that accounts for PTC by solving second order moments.

After choosing the modeling approach, the choice of the numerical schemes needs to be addressed. In fact, for the Eulerian simulation of disperse phase flows, accurate and robust numerical methods are mandatory, as they can highly influence the captured physics of the flow [25]. More specifically, the two closures in question yield hyperbolic (Gaussian) or weakly hyperbolic systems (MK), which present some difficulties, especially on unstructured meshes and in the presence of void regions and singularities. Furthermore, moment methods require that the numerical scheme satisfies the realizability condition (every set of moments has to be associated with a positive NDF) in each cell. This realizability condition translates into the positivity of mass or of the internal energy, for example. To fulfill these conditions, one can use kinetic schemes [26]: by using the exact solution in time of the underlying kinetic description such schemes are intrinsically realizable. This type of scheme was adapted to moment methods for polydispersion [27] or PTC but it is nowadays limited to

second order of accuracy. On the other hand, in the literature, several high order numerical schemes can be found for the resolution of hyperbolic system of equations. For example, the two step Taylor Galerkin scheme of Colin (TTGC) [28] used in the AVBP code achieves third order in space and time on unstructured grids, for very regular solutions. Unfortunately for general solutions, the dispersive character of these centered schemes imposes the use of empirical artificial diffusion, which needs to be manually tuned, decreasing as a result the order of convergence without eventually ensuring the generic robustness.

In order to meet all these properties, i.e. realizability preservation and high order of accuracy on unstructured mesh, a new class of Runge-Kutta Discontinuous Galerkin scheme is used [5]. Based on the work of Zhang and Shu [7] and Zhang et al. [6] on positivity preserving and maximum principle satisfying schemes, this scheme is built to preserve the realizability conditions without degrading the order of the method.

The main contribution of this work is to apply one of the latest developments in the field of numerical methods, a realizable new class of DG scheme with a convex projection strategy, to physical models taking into account the key part of the transport of the disperse phase flow which is the convective term. This scheme is tested and compared, qualitatively by means of snapshots of the particles number density and quantitatively through a segregation study, to a second order realizable MUSCL/HLL finite volume scheme [3]. The results of these two schemes are compared also to the Lagrangian result which is considered to be the physical reference. The ability of Eulerian models to properly predict segregation without capturing the comprehensive details of PTC for moderate Stokes numbers is also highlighted.

The content of this paper is the following: the second section presents the modeling approach with the two closures (MK and Gaussian). The numerical schemes (RKDG and MUSCL/HLL) are described in the third section. Finally, the 2-D numerical results for the test cases based on the two different closures are presented in the fourth section. The quality of the results is evaluated by comparing the snapshots of the number density for the different schemes and by investigating the evolution of the segregation with time. Finally, a more realistic quality/CPU time comparison between the two numerical schemes is performed.

2. KINETIC-EULERIAN MODELING

2.1 Statistical Approach of the Particle Repartition

The formalism presented for the first step of modeling is called the kinetic approach, since it was inspired by the kinetic theory of gases. A statistical description of the disperse phases is used through a NDF $f(t, \overrightarrow{\mathbf{x}}, \boldsymbol{\xi})$, where t is the time, $\overrightarrow{\mathbf{x}}$ the position and $\boldsymbol{\xi}$ the internal phase space. The dimension of the phase space is related to the number of internal coordinates necessary to describe the physics of one particle. The sole choice of the phase space is strongly related to the physics one wants to describe. For example, if we consider that the particles are spherical, $\boldsymbol{\xi} = (\overrightarrow{\mathbf{c}}, S, T)$ is the phase space composed of velocity, size and temperature. In this case, the statistical approach leads to a mesoscopic description given by the Williams-Boltzmann equation [11]:

$$\partial_t f + \partial_{\overrightarrow{\mathbf{x}}} \cdot (\overrightarrow{\mathbf{c}} f) + \partial_{\overrightarrow{\mathbf{c}}} \cdot (\overrightarrow{\mathbf{F}} f) + \partial_S (R_S f) + \partial_T (K f) = \Gamma + Q \tag{1}$$

The first two terms are the free transport of the discrete phase, $\overrightarrow{\mathbf{F}} = d_t \overrightarrow{\mathbf{c}}$ is the acceleration of the particles (drag force applied on the particles per unit mass) due to the presence of the underlying continuous phase, $R_S = d_t S$ is the evaporation rate (rate of change of the particle size due to evaporation), $K = d_t T$ is the rate of change of the particle temperature due to heat transfer and the source terms Γ, Q are the collision and secondary break-up operators.

For the sake of simplicity and since our focus is on the free transport and drag terms, we will not take into account evaporation, heat transfer, collisions and secondary break-up. For more details on the modeling strategies of these terms refer to de Chaisemartin [29, 4], Dufour et al. [22], Laurent et al. [30] and Doisneau et al. [31] and references therein . Furthermore, we will consider a monodisperse phase (all particles have the same size) eventhough polydispersity could be included through a Multi-Fluid size phase space discretization with various levels of size and moment conservation equations in each section [1, 2, 29, 4, 27, 31].

The drag term is modeled by a Stokes law (as an illustration), so that the acceleration is equal to the ratio of the velocity difference between the continuous phase and the particle to a characteristic particle relaxation time

$$\tau_p = \frac{\rho_l d_p^2}{18\mu_g} \tag{2}$$

where ρ_l is the particle material density, d_p its diameter and μ_g the dynamic viscosity of the carrying phase. This law is suitable in the case of moderate Reynolds number, but the study presented hereafter can be generalized for other models of the drag term.
The Stokes number is defined as the ratio of the particle relaxation time to a characteristic time of the continuous phase. The resulting acceleration of the particles is therefore:

$$\overrightarrow{F} = \frac{\overrightarrow{\mathbf{u}_g} - \overrightarrow{\mathbf{c}}}{\tau_p} \tag{3}$$

The resulting simplified equation reads:

$$\partial_t f + \partial_{\overrightarrow{\mathbf{x}}} \cdot (\overrightarrow{\mathbf{c}} f) + \partial_{\overrightarrow{\mathbf{c}}} \cdot \left(\frac{\overrightarrow{\mathbf{u}_g} - \overrightarrow{\mathbf{c}}}{\tau_p} f \right) = 0 \tag{4}$$

2.2 The Eulerian Approach and the Method of Moments

After integrating eqn (4) over the phase space, one gets a system of moment equations. In a two-dimensional space, the general equation on the moments is:

$$\partial_t M_{i,j} + \partial_x (M_{i+1,j}) + \partial_y (M_{i,j+1}) = \frac{i(U_g M_{i-1,j}) + j(V_g M_{i,j-1}) - (i+j) M_{i,j}}{\tau_p} \tag{5}$$

where the general $(i+j)^{th}$ order moment in velocity is $M_{i,j} = \int U^i V^j f dU dV$ and U and V are respectively the x and y component of the velocity. For example the 0^{th} order moment, common to all the phase variables, is equal to the number density ρ.
This system is not closed: actually for every set of moments of order N which contains the moments of order $(i+j) \leq N$, moments of order $N+1$ are needed to describe the fluxes in physical space [3]. In order to close this system, one then needs to provide:

- the moment set of order N+1, and
- a closure relationship which allows to find the unknown fluxes (assumptions on the velocity distribution for example).

One can find several models based on different closures in the literature, such as the monokinetic (MK) [1], the Gaussian divided into isotropic Gaussian [2] and anisotropic Gaussian (AG) [32, 3], the quadrature based moment methods [23, 20] and the multi-Gaussian [33]. The choice of the closure is imposed by the physics one needs to describe.
In the following, we study two models base on the MK and the Gaussian closures.

2.2.1 Monokinetic Closure

In turbulent flow, the dynamics of the disperse phase can be classified by its Stokes number relative to the Kolmogorov time scale. In the case of low Stokes number (less than one) where we do not have significant PTC, high segregation effects occur which leads to stiff accumulation regions along with vacuum generation in their vicinity. These effects can be reproduced by the MK closure [1]. This near equilibrium assumption is known as the hydrodynamic limit for the solution of the Boltzmann equation in the kinetic theory (the NDF is the generalized Maxwell Boltzmann closure with zero temperature). This NDF is assumed to write $f(t, \overrightarrow{\mathbf{x}}, \overrightarrow{\mathbf{c}}) = \rho(t, \overrightarrow{\mathbf{x}}) \delta(\overrightarrow{\mathbf{c}} - \overrightarrow{\mathbf{u}}(t, \overrightarrow{\mathbf{x}}))$, where $\overrightarrow{\mathbf{u}}(t, \overrightarrow{\mathbf{x}})$ is the mean velocity of the disperse phase. The system of moments closes at first order in moments and we get therefore the following system:

$$\begin{cases} \partial_t \rho + \partial_{\overrightarrow{\mathbf{x}}} \cdot (\rho \overrightarrow{\mathbf{u}}) = 0 \\ \\ \partial_t (\rho \overrightarrow{\mathbf{u}}) + \partial_{\overrightarrow{\mathbf{x}}} \cdot (\rho \overrightarrow{\mathbf{u}} \otimes \overrightarrow{\mathbf{u}}) = \dfrac{\rho(\overrightarrow{\mathbf{u}_g} - \overrightarrow{\mathbf{u}})}{\tau_p} \end{cases} \tag{6}$$

This model is for example used in the field of spray dynamics for combustion applications [29, 34] and in the field of solid propellant combustion [31]. This model correctly reproduces the formation of depletion zones and accumulations regions but it does not take into consideration PTC, which occur for high inertial particles, since they can not be capture by the single Dirac δ-function used for the velocity distribution in the model. Another constraint of this model is that it does not preserve kinetic energy [35, 36] .

Among the different closures known in the literature and which deal with the coexistence of different velocities at PTC locations, the Gaussian closure [32, 3] is chosen here.

2.2.2 Gaussian Closure

Under the assumption of anisotropic Gaussian closure (AG), the NDF is assumed to write $f(t,\overrightarrow{\mathbf{x}},\overrightarrow{\mathbf{c}}) = \rho(t,\overrightarrow{\mathbf{x}})\mathcal{N}(\overrightarrow{\mathbf{c}}-\overrightarrow{\mathbf{u}}(t,\overrightarrow{\mathbf{x}}),\mathbf{\Sigma}(t,\overrightarrow{\mathbf{x}}))$ where $\mathcal{N}$ is a joint Gaussian distribution of center $\overrightarrow{\mathbf{u}}$ and covariance matrix $\mathbf{\Sigma} = (\sigma_{ij})$:

$$\mathcal{N}(\overrightarrow{\mathbf{c}}-\overrightarrow{\mathbf{u}},\mathbf{\Sigma}) = \frac{|\mathbf{\Sigma}|^{-1/2}}{(2\pi)^{N_d/2}}\exp\left(-\frac{1}{2}(\overrightarrow{\mathbf{c}}-\overrightarrow{\mathbf{u}})^T\mathbf{\Sigma}^{-1}(\overrightarrow{\mathbf{c}}-\overrightarrow{\mathbf{u}})\right) \tag{7}$$

The resulting system reads:

$$\begin{cases} \partial_t\rho + \partial_{\overrightarrow{\mathbf{x}}}\cdot(\rho\overrightarrow{\mathbf{u}}) = 0 \\ \partial_t(\rho\overrightarrow{\mathbf{u}}) + \partial_{\overrightarrow{\mathbf{x}}}\cdot(\rho\overrightarrow{\mathbf{u}}\otimes\overrightarrow{\mathbf{u}}+\mathbf{P}) = \dfrac{\rho(\overrightarrow{\mathbf{u}_g}-\overrightarrow{\mathbf{u}})}{\tau_p} \\ \partial_t(\rho\mathbf{E}) + \partial_{\overrightarrow{\mathbf{x}}}\cdot((\rho\mathbf{E}+\mathbf{P})\vee\overrightarrow{\mathbf{u}}) = \dfrac{\rho(\overrightarrow{\mathbf{u}_g}\vee\overrightarrow{\mathbf{u}}-2\mathbf{E})}{\tau_p} \end{cases} \tag{8}$$

where $\vee$ denotes the symmetric tensor outer product[1], the total energy tensor $\mathbf{E}$ is given by the equation of state $\mathbf{E} = \frac{1}{2}\overrightarrow{\mathbf{u}}\otimes\overrightarrow{\mathbf{u}} + \frac{\mathbf{P}}{2\rho}$ and the anisotropic pressure tensor is $\mathbf{P} = \rho\mathbf{\Sigma}$.
The rational use of such an approach is detailed in [3].

In this work, we start with the simplified version of this system where an isotropic pressure is considered, which leads to an isotropic Gaussian closure based model. In this case, by applying the trace operator on the last equation of system (8) we get a scalar conservation of energy instead of the tensorial energy equation where $\mathcal{E}$ is the trace of the energy matrix. The resulting simplified system reads:

$$\begin{cases} \partial_t\rho + \partial_{\overrightarrow{\mathbf{x}}}\cdot(\rho\overrightarrow{\mathbf{u}}) = 0 \\ \partial_t(\rho\overrightarrow{\mathbf{u}}) + \partial_{\overrightarrow{\mathbf{x}}}\cdot(\rho\overrightarrow{\mathbf{u}}\otimes\overrightarrow{\mathbf{u}}+\mathbf{P}) = \dfrac{\rho(\overrightarrow{\mathbf{u}_g}-\overrightarrow{\mathbf{u}})}{\tau_p} \\ \partial_t(\rho\mathcal{E}) + \partial_{\overrightarrow{\mathbf{x}}}\cdot((\rho\mathcal{E}+\mathcal{P})\cdot\overrightarrow{\mathbf{u}}) = \dfrac{\rho(\overrightarrow{\mathbf{u}_g}\cdot\overrightarrow{\mathbf{u}}-2\mathcal{E})}{\tau_p} \end{cases} \tag{9}$$

with,

$$\mathcal{E} = tr(\mathbf{E}) = \frac{1}{2}\left|\overrightarrow{\mathbf{u}}\right|^2 + \sigma, \tag{10}$$

$$\mathbf{P} = \mathcal{P}\mathbf{I} = \rho\sigma\mathbf{I} \tag{11}$$

The free transport part of systems (6) and (9) are respectively identical to the Pressureless Gas Dynamics (PGD) system and the Euler system of equations. The PGD system is weakly hyperbolic (in the sense that the Jacobian matrix is triangulable but non-diagonalizable) and it can generate δ-shocks [35]. These singularities are difficult to handle by numerical schemes, especially without globally degenerating the order of accuracy. In addition, special care needs to be taken, in order to

[1] The symmetric tensor outer product acts on a symmetric k-tensor and a symmetric l-tensor by symmetrizing the $(k+l)$-tensor that is their usual tensor outer product [32].

maintain the realizability condition so that every pair of moment $(\rho, \rho\vec{\mathbf{u}})$ is associated with a positive NDF. The positivity of the number density ρ should therefore be preserved. In addition, a physical convex contraint is applied to the velocity $\vec{\mathbf{u}}$ so that it would respect a maximum principle. Similarly, for the Euler-like system, which is hyperbolic, the realizability conditions should be respected: the density and the pressure have to stay positive.

In both models, the realizability conditions define a realizable space, which is known to be a convex space [37]. This realizable space defines the constraints of the numerical scheme. In addition, a high order robust numerical method is needed in order to capture the fine structures appearing in the solution and to reproduce the large variations that might be encountered in the density field (going from vacuum zones to high concentration regions) without inducing spurious oscillations. To sum up, the numerical scheme should be:

- **accurate** to be able to reproduce the large variations of the density,
- **realizable** in order to maintain a physical solution,
- applicable to **unstructured meshes** needed to simulate disperse phase flows in real configurations including complex geometries,
- as **cost effective** as possible, otherwise it would not be suitable for industrial use,
- **parameter free**: for example no need for artificial viscosities to stabilize the scheme and suppress spurious oscillations that can result near high gradients.

To achieve these goals, a new class of Discontinuous Galerkin method is a promising approach.

3. NUMERICAL SCHEMES

In this section we present two numerical schemes. The first one, which is the subject of our study, is a convex state preserving Runge-Kutta discontinous Galerkin method (RKDG) and the second one, which is introduced for the sake of comparison, is a realizable second order finite volume MUSCL/HLL scheme. Because this reference finite volume scheme is limited to second order, we are only considering a second order version of the RKDG method. It is however known that it can be generalized to arbitrary high-order accuracy in space and time, see [8]. Also, for simplicity, a second order Strang splitting strategy is used hereafter to integrate the right hand side source term [38]. The source term ODE resulting from the splitting is afterward solved exactly, thanks to its simple form. Nevertheless, one should note that in a very high order context, it is also possible to solve the entire system including source terms within the discontinuous Galerkin framework [39].

3.1 Convex Constraints Preserving Discontinuous Galerkin Formulation

The high order unstructured numerical scheme used to solve the convective part of the systems of equations resulting from the modeling procedure in the previous section is presented hereafter. The method used is a Discontinuous Galerkin (DG) scheme based on the classical DG formulation [40] and evolved to satisfy the realizability constraints by the application of the maximum principle and a positivity preservation technique [7, 6]. The extension of this framework to the case of weakly hyperbolic equations (PGD system) was initiated by Larat et al. [5]. In this first subsection, the general framework of the realizability constraints preservation is introduced in one dimension of space. Extension to two dimensional computation is then explained in the second subsection. Furthermore, this extension to 2-D problems can be generalized to any higher number of spatial dimensions.

3.1.1 Scheme in One-Dimension of Space

The general form of the system of conservation laws in one dimension is:

$$\partial_t \mathbf{W} + \partial_x \boldsymbol{\mathcal{F}}(\mathbf{W}) = 0, \quad x \in [0,1]; t \in [0, T_s] \tag{12}$$

where $\mathbf{W}(x,t)$ is the unknown state of moments and $\boldsymbol{\mathcal{F}}(\mathbf{W})$ the conservative flux.
For the PGD and Euler systems we have respectively:

$$\mathbf{W}_{PGD} = (\rho, \rho u), \quad \boldsymbol{\mathcal{F}}_{PGD} = (\rho u, \rho u^2) \tag{13}$$

$$\mathbf{W}_{Euler} = (\rho, \rho u, \rho E), \quad \boldsymbol{\mathcal{F}}_{Euler} = (\rho u, \rho u^2 + P, (\rho E + P)u) \tag{14}$$

We consider an initial boundary value problem (IBVP) with initial condition $\mathbf{W}_0$ and periodic boundary conditions:

$$\mathbf{W}(x,0) = \mathbf{W}_0(x), \quad \forall x \in [0,1] \tag{15}$$
$$\mathbf{W}(0,t) = \mathbf{W}(1,t), \quad \forall t \in [0,T_s] \tag{16}$$

First, the computational domain is divided into $N = \frac{1}{h}$ sub-intervals C_i, see Figure 1.

$$C_i =]x_{i-\frac{1}{2}}, x_{i+\frac{1}{2}}[\tag{17}$$

where,

$$x_{i-\frac{1}{2}} = \frac{(i-1)}{N}, \quad x_i = \frac{(i-1/2)}{N}, \quad x_{i+\frac{1}{2}} = \frac{i}{N}, \quad i = 1, ..., N \tag{18}$$

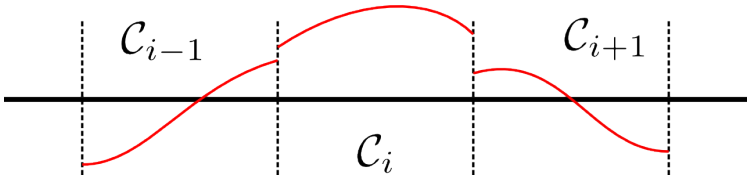

Figure 1. Space discretization for DG scheme

For the sake of clarity a structured mesh is used, but a similar work can be done for an unstructured discretization in a more general context. Then, for a method of order $k+1 \in \mathbb{N}^*$, $\varphi_i^j(x)$ are $k+1$ basis functions, polynomials of order k in C_i, for $j = 1, ..., k+1$. The L^2 scalar products of the φ_i^js over C_i give the mass matrix $\mathcal{M}$:

$$(\mathcal{M})_{jl} = \int_{C_i} \varphi_i^j(x)\varphi_i^l(x)\mathrm{d}x,$$

which becomes diagonal under the choice of a suitable orthogonal basis. Next, according to classical DG formulation, the numerical solution $\mathbf{W}_h$ is the unique solution within the functional space spanned by the φ_i^js of the variational formulation of (12) in this functional space:

$$\mathbf{W}_h(x,t) = \sum_{i,j} \mathbf{W}_i^j(t)\varphi_i^j(x)\chi_{C_i}(x) \tag{19}$$

where χ_{C_i} is C_i indicator function, and

$$\int_{C_i} \left(\partial_t \mathbf{W}_h + \partial_x \boldsymbol{\mathcal{F}}(\mathbf{W}_h)\right)\varphi_i^j(x)\mathrm{d}x = 0, \quad \forall i = 1, \ldots, N, \forall j = 1, \ldots, k+1. \tag{20}$$

By combining the two last equations and integrating by part, we get the following DG semi-discretization in space:

$$|C_i|(\boldsymbol{\mathcal{M}}_{jl})d_t\mathbf{W}_i^l + \left(\boldsymbol{\mathcal{F}}^*_{i+\frac{1}{2}}\varphi_i^j(x_{i+\frac{1}{2}}) - \boldsymbol{\mathcal{F}}^*_{i-\frac{1}{2}}\varphi_i^j(x_{i-\frac{1}{2}})\right) = \int_{C_i} \boldsymbol{\mathcal{F}}(\mathbf{W}_h(x,t))\partial_x\varphi_i^j\mathrm{d}x, \quad \forall i = 1, ..., N; \forall j = 1, ..., k, \tag{21}$$

where $\boldsymbol{\mathcal{F}}^*_{i+\frac{1}{2}}$ is a chosen numerical flux at cell interface $x_{i+\frac{1}{2}}$.

Once this is done, one obtains a set of ordinary differential equations (ODE) for the degrees of freedom (DOF) $\mathbf{W}_i^j(t)$ which need to be solved in time. Typically, one would use a $(k+1)^{th}$ order accurate Runge-Kutta (RK) integrator, for example a $(k+1)$-step Runge-Kutta. However, it is known that for an order of accuracy higher than 4, the $(k+1)^{th}$ order accurate $(k+1)$-step Runge-Kutta does not involve only strictly positive weights and one would therefore loose the convexity preservation needed for realizability. Fortunately, there exist a familly of Strong Stability Preserving (SSP) [41] time integrators which respect this constraint and this is what we are going to use. The

following explains the realizability preservation within the context of a first order forward Euler time integration, having in mind the obvious generalization to any SSP method.

Let us now explain the preservation of the convex constraint of realizability by the DG scheme. By summing eqn (21) over all the DOF j of a given cell C_i, one obtains the equation of evolution of the cell mean value:

$$\overline{\mathbf{W}}_i^{n+1} = \overline{\mathbf{W}}_i^n - \frac{\Delta t}{|C_i|}\left(\boldsymbol{\mathcal{F}}^*_{i+\frac{1}{2}} - \boldsymbol{\mathcal{F}}^*_{i-\frac{1}{2}}\right). \tag{22}$$

Now, because $\mathbf{W}_h$ is a k^{th} order polynomial in C_i, the following Gauss-Lobatto quadrature is exact, when m is such that $k \leq 2m-3$:

$$\overline{\mathbf{W}}_i = \frac{1}{|C_i|}\int_{C_i} \mathbf{W}_h(x,t^n)\mathrm{d}x = \sum_{q=1}^{m} \omega_q \mathbf{W}_h(x_q,t^n). \tag{23}$$

In 1D, it is known that the m Gauss-Lobatto quadrature points x_q, $q = 1,...,m$ have strictly positive weights ω_q.

Next, the balance of the numerical fluxes $\boldsymbol{\mathcal{F}}^*_{i+\frac{1}{2}} = \boldsymbol{\mathcal{F}}^*(x_{i+\frac{1}{2}})$ and $\boldsymbol{\mathcal{F}}^*_{i-\frac{1}{2}} = \boldsymbol{\mathcal{F}}^*(x_{i-\frac{1}{2}})$ entering the cell C_i is split into a sum of balances of numerical fluxes at two neighboring quadrature points:

$$\boldsymbol{\mathcal{F}}^*_{i+\frac{1}{2}} - \boldsymbol{\mathcal{F}}^*_{i-\frac{1}{2}} = \boldsymbol{\mathcal{F}}^*(x_{i+\frac{1}{2}}) - \boldsymbol{\mathcal{F}}^*(x_{i-\frac{1}{2}}) = \sum_{q=0}^{m}\left(\boldsymbol{\mathcal{F}}^*(x_{q+1}) - \boldsymbol{\mathcal{F}}^*(x_q)\right). \tag{24}$$

The set of m quadrature points has been implicitly extended to $q = 0,...,m+1$ where x_0 and

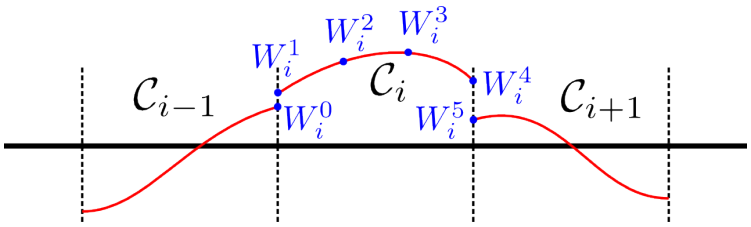

Figure 2. Quadrature points on the cell C_i

x_{m+1} are respectively the coordinates of the right and left quadrature point on the left and right neighboring cell, see Figure 2. Finally, by combining the three above equations, one obtains the updating equation:

$$\overline{\mathbf{W}}_i^{n+1} = \sum_{q=0}^{m} \omega_q \left(\mathbf{W}_h(x_q,t^n) - \frac{\Delta t}{\omega_q |C_i|}\left(\boldsymbol{\mathcal{F}}^*(x_{q+1}) - \boldsymbol{\mathcal{F}}^*(x_q)\right)\right), \tag{25}$$

which looks like a convex combination of abstract first order updates, because $\omega_q > 0, \forall q$.

Now, we define what we mean by *realizability preserving numerical flux* for a first order finite volume scheme.

Definition 1 *If $\mathbf{W}_{i-1}^n$, $\mathbf{W}_i^n$ and $\mathbf{W}_{i+1}^n$ are three neighboring realizable states at time step n, the numerical flux $\boldsymbol{\mathcal{F}}^*$ is called **realizability preserving** if the updated mean state in cell C_i*

$$\overline{\mathbf{W}}_i^{n+1} = \mathbf{W}_i^n - \frac{\Delta t}{|C_i|}\left(\boldsymbol{\mathcal{F}}^*_{i+\frac{1}{2}}(\mathbf{W}_{i+1}^n, \mathbf{W}_i^n) - \boldsymbol{\mathcal{F}}^*_{i-\frac{1}{2}}(\mathbf{W}_i^n, \mathbf{W}_{i-1}^n)\right) \tag{26}$$

is realizable under the classical CFL condition for first order finite volume schemes.

In the case of the PGD system or the Euler system, there exist many such realizability preserving fluxes. Among them one can cite the familly of HLL solvers or even exact Godunov solvers. In this paper we consider the Lax-Friedrichs flux, which can be viewed as a particular HLL approximate Riemann solver. Then, the higher order update in eqn (25) is also realizability preserving when

- the numerical flux $\boldsymbol{\mathcal{F}}^*$ is realizability preserving,

- the quadrature states $\mathbf{W}_q^n = \mathbf{W}_h^n(x_q)$ are realizable,
- the following constrained CFL condition is provided:

$$\frac{\Delta t.\alpha_i}{|C_i|} \leq \min_q \omega_q, \tag{27}$$

where α_i is greater than the absolute value of the eigenvalues of the Jacobian of the flux at all the quadrature points x_q, $q = 0, \ldots, m+1$.

At second order in 1D, this last CFL constraint is $\frac{1}{2}$, which is exactly the same CFL constraint as for second order finite volume schemes. In the next subsection we generalize these conditions to 2D and the CFL constraint for second order accuracy becomes $\frac{1}{3}$. It is also important to notice that the Gauss-Lobatto quadrature does not have to be necessarily used in the evaluation of the overall updates in eqn (21). One can use any accurate enough quadrature to estimate the right hand side integral. However, realizability at the Gauss-Lobatto quadrature points will certainly ensure realizability of the mean value at next time step.

A delicate point still needs to be adressed to finish our proof. The initial condition is supposed to be physical and thus realizable everywhere, in particular at the quadrature points. By using a realizability preserving numerical flux and keeping the restricted CFL condition (27), we obtain realizable mean values in each cell C_i for the first time step. But nothing ensures the solution to be now realizable at every quadrature point. Fortunately, because the space of realizable moments $\mathcal{S}$ is convex, for each non-realizable quadrature state $\mathbf{W}_i^q = \mathbf{W}_h(x_q)$ there exist a unique $\theta_q \in [0,1]$ such that $\widetilde{\mathbf{W}}_i^q = \theta_q \mathbf{W}_i^q + (1-\theta_q)\overline{\mathbf{W}}_i$ lies on the boundary of $\mathcal{S}$, see Figure 3. The numerical solution is then

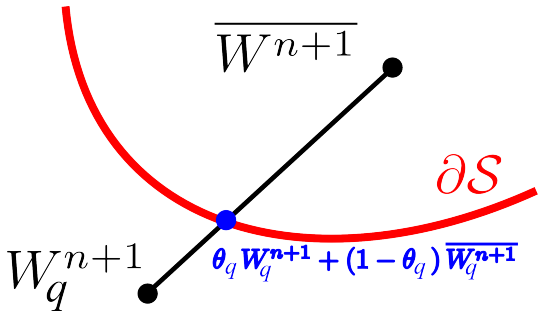

Figure 3. A space projection in cell C_i, associating for any quadrature state $\mathbf{W}_q^{n+1}$ lying outside the space of constraints, a state $\widetilde{\mathbf{W}}_q^{n+1}$ at the boundary $\partial\mathcal{S}$ of this space

redefined as:

$$\widetilde{\mathbf{W}}_h(x, t^{n+1}) = \theta_i(\mathbf{W}_h(x, t^{n+1}) - \overline{\mathbf{W}}_i^{n+1}) + \overline{\mathbf{W}}_i^{n+1}, \quad \theta_i = \min_{q=1,..,m} \theta_q, \tag{28}$$

This space projection has the following properties:

- the cell mean value is obviously conserved,
- it is shown in [8] that the accuracy of the scheme is preserved for regular solutions.

$\widetilde{\mathbf{W}}_h$ is finally a $(k+1)^{th}$ order approximation of $\mathbf{W}_h$ which respects the convex constraints at all quadrature points, which can be used for next time step and the scheme can go on.

3.1.2 Extention to 2 – D

The 2-D domain is tesselated into triangles. Let T_i be a triangle of the mesh and j a DOF of T_i with its associated k^{th} order basis function $\varphi_{T_i}^j$. The conservative flux is $\mathcal{F}(\mathbf{W}) = (\mathbf{f}(\mathbf{W}), \mathbf{g}(\mathbf{W}))$ where for the PGD and Euler system we have respectively:

$$\mathbf{W}_{PGD} = \rho \begin{pmatrix} 1 \\ u \\ v \end{pmatrix}, \mathcal{F}_{PGD} = \rho \left(\begin{pmatrix} u \\ u^2 \\ uv \end{pmatrix}, \begin{pmatrix} v \\ uv \\ v^2 \end{pmatrix} \right) \tag{29}$$

$$\mathbf{W}_{Euler} = \rho \begin{pmatrix} 1 \\ u \\ v \\ \mathcal{E} \end{pmatrix}, \mathcal{F}_{Euler} = \left(\begin{pmatrix} \rho u \\ \rho u^2 + \mathcal{P} \\ \rho uv \\ (\rho\mathcal{E} + \mathcal{P})u \end{pmatrix}, \begin{pmatrix} \rho v \\ \rho uv \\ \rho v^2 + \mathcal{P} \\ (\rho\mathcal{E} + \mathcal{P})v \end{pmatrix} \right) \tag{30}$$

The numerical flux $\mathcal{F}^*(\mathbf{W}_{ext}, \mathbf{W}_{int}, \overrightarrow{\mathbf{n}})$ is supposed to be **realizability preserving**. $\mathbf{W}_{ext}$ and $\mathbf{W}_{int}$ denote states on both sides of the considered edge of normal $\overrightarrow{\mathbf{n}}$. Then the differential system reads:

$$|T_i|(\mathcal{M}_{jl})d_t\mathbf{W}^l_{T_i} + \int_{\partial T} \mathcal{F}^* \left(\mathbf{W}_{ext}(s), \mathbf{W}_{int}(s), \vec{\mathbf{n}}(s)\right) \varphi^j_{T_i}(s)ds = \int_{T_i} \mathcal{F}(\mathbf{W}(x,t)) \cdot \overrightarrow{\nabla\varphi^j_{T_i}} \mathrm{d}x \tag{31}$$

After summing over all the degrees of freedom j of T_i and discretizing in time, we get the equation of the evolution of the mean value in T_i:

$$\overline{\mathbf{W}}^{n+1}_{T_i} = \overline{\mathbf{W}}^{n}_{T_i} - \int_{\partial T} \mathcal{F}^* \left(\mathbf{W}_{ext}(s), \mathbf{W}_{int}(s), \vec{\mathbf{n}}(s)\right) ds \tag{32}$$

where the right contour integral is estimated using the appropriate Gauss quadrature. The main dif-

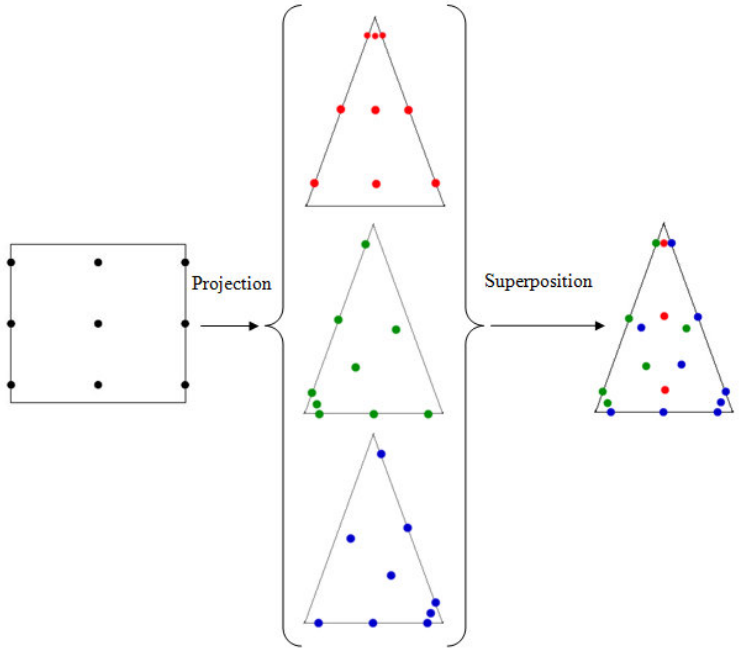

Figure 4. The quadrature points on the triangle for k=2 resulting from the superposising of the three projections (inspired by Zhang el al. [6])

ficulty in the extension of the 1-D scheme to two dimensions is to find a quadrature rule which is exact for polynomial of order k, has strictly positive quadrature weights and includes in its quadrature points the Gauss quadrature points used to integrate the numerical fluxes on ∂T. If such a quadrature exists, in a similar way to the 1D case the mean value update (32) can be recast into a convex combination of states at interior quadrature points and formal first order updates at edges Gauss quadrature points [6]. Under a certain CFL condition, $\overline{\mathbf{W}}^{n+1}_{T_i}$ is then realizable if $\mathbf{W}_h$ is realizable at all the quadrature points, what can be ensured in the same way as in the one dimensional case. A quadrature with such properties exists naturally on quadrangles through a tensor product of the considered Gauss quadrature for the edges in one direction and an accurate enough ($2m - 3 \geq k$) Gauss-Lobatto quadrature in the other direction. A projection mapping the top edge of the quadrangle onto one vertex of the triangle and the other edges onto the three edges of the triangle will then give a set of quadrature points at desired accuracy, with strictly positive quadrature weights and which coincide with the Gauss quadrature points on two of the three edges. By this mean, three projections are defined and by superposing the three resulting sets we obtain the sought quadrature. Figure 4 illustrates the construction of such a set of quadrature points in a very high order framework. The represented set of quadrature points works for polynomials of order 2 and 3: it allows for third and forth order numerical methods in space and eventually involves 18 quadrature points. However, in the second order case, *ie.* linear representation of the solution, only 6 quadrature points are required: 2 per edges.

Finally, it can be shown that for this special quadrature points construction, the realizability constraint is

$$\frac{\alpha_{T_i}\Delta t\,|\partial T_i|}{|T_i|} \leq \frac{2}{3}\omega_1^{G-L}, \tag{33}$$

where α_{T_i} is still an overestimation of the eigenvalues of the Jacobian of the flux at all the considered quadrature points for a given triangle T_i, $|T_i|$ is the perimeter of T_i and ω_1^{G-L} is the smallest weight (always on the edges of the interval) of the considered Gauss-Lobatto quadrature. At second order, we will use 2 points with weight $\frac{1}{2}$, which means a $\frac{1}{3}$ CFL constraint.

3.2 Realizable MUSCL/HLL Scheme

In order to assess the DG approach, we compare it to a finite volume scheme of the same order. Here, a realizable second order MUSCL/HLL [3] has been chosen. It is obtained using the MUSCL strategy [9] with a linear conservative reconstruction of the primitive variable ($\boldsymbol{\mathcal{U}} = \left(\rho, \overrightarrow{\mathbf{u}}\right)$ for the PGD system and $\boldsymbol{\mathcal{U}} = \left(\rho, \overrightarrow{\mathbf{u}}, \sigma\right)^T$ for Euler system) within each cell in order to calculate the interface values. This reconstruction should be conservative. The evaluation of the fluxes is then done with a first order flux using the reconstructed values at the interface. Multi-dimensional problems are sloved by a dimensional splitting strategy. The time integration is done by means of a 2nd order Runge-Kutta method.
In the following, the reconstruction, the slope limitation and the flux evalution strategies are shown for the 2-D scheme in the x-direction, for more details one may refer to the work of Vié et al. [24, 3].

3.2.1 Conservative Reconstruction

The linear reconstruction proposed in [3] is based on central moments. The main objective of this reconstruction strategy is to ensure the realizability of the moment set. The cell reconstructed variables $\tilde{\boldsymbol{\mathcal{U}}}$ are obtained by the limited linear reconstruction based on the corrected cell value $\overline{\boldsymbol{\mathcal{U}}}$ for each reconstructed variable:

$$\tilde{\boldsymbol{\mathcal{U}}}_i(x) = \overline{\boldsymbol{\mathcal{U}}}_i + \mathcal{D}_{\boldsymbol{\mathcal{U}}}(x - x_i) \tag{34}$$

where for the PGD and Euler systems we have respectively:

$$\overline{\boldsymbol{\mathcal{U}}}_{i,PGD} = (\overline{\rho}_i, \overline{u}_i, \overline{v}_i)^T, \quad \mathcal{D}_{\boldsymbol{\mathcal{U}},PGD} = (D_{\rho_i}, D_{u_i}, D_{v_i})^T \tag{35}$$

$$\overline{\boldsymbol{\mathcal{U}}}_{i,Euler} = (\overline{\rho}_i, \overline{u}_i, \overline{v}_i, \overline{\sigma}_i)^T, \quad \mathcal{D}_{\boldsymbol{\mathcal{U}},Euler} = (D_{\rho_i}, D_{u_i}, D_{v_i}, D_{\sigma_i})^T \tag{36}$$

The corrected cell values are one of the main differences between the scheme used in this work and the classical reconstruction strategies of MUSCL schemes [42]. These corrected cell values are imposed by the conservation of the cell value for each moment in order to ensure that the fluxes will not affect the realizability [24]:

$$M_{kl} = \frac{1}{\Delta x}\int_{x_{i-1/2}}^{x_{i+1/2}} \tilde{M}_{kl,i}(x)\mathrm{d}x \tag{37}$$

where $k + l \leq 1$ for the PGD system and $k + l \leq 2$ for the Euler system. Finally the corrected cell values are:

$$\overline{\rho}_i = \rho_i, \qquad \overline{u}_i = u_i - \frac{D_{\rho_i}D_{u_i}}{\rho_i}\frac{\Delta x^2}{12}, \qquad \overline{v}_i = v_i - \frac{D_{\rho_i}D_{v_i}}{\rho_i}\frac{\Delta x^2}{12} \tag{38}$$

$$\overline{\sigma}_i = \sigma_i - \frac{\Delta x^2}{12}\left(\frac{D_{u_i}^2 + D_{v_i}^2}{2}\right)\left(1 + \frac{\Delta x^2}{12}\frac{D_{\rho_i}^2}{\rho_i^2}\right) - \frac{\Delta x^2}{12}\frac{D_{\rho_i}D_{\sigma_i}}{\rho_i} \tag{39}$$

The last step of this reconstruction is the slope evaluation.

3.2.2 Slope Limitation

Since the slopes can generate unrealizable corrected cell values, the slope evaluation is complex but mandatory to ensure the positivity of the density, the variance (in case of Euler system) and to force a maximum principle of the variables to guarantee robustness. A minmod limiter with a positivity constraint is first applied to the density:

$$D_{\rho_i} = \frac{1}{2}\left(\text{sign}(\rho_{i+1}-\rho_i)+\text{sign}(\rho_i-\rho_{i-1})\right)\min\left(\frac{\rho_{i+1}-\rho_i}{\Delta x}, \frac{\rho_i-\rho_{i-1}}{\Delta x}, \frac{2\rho_i}{\Delta x}\right) \tag{40}$$

In case of the PGD system, a slope limiter is applied to the velocities:

$$D_{u_i,PGD} = \frac{1}{2}\left(\text{sign}(u_{i+1}-u_i)+\text{sign}(u_i-u_{i-1})\right)\min\left(\frac{|u_{i+1}-u_i|}{\Delta x\left(1-\frac{D_{\rho_i}}{\rho_i}\frac{\Delta x}{6}\right)}, \frac{|u_i-u_{i-1}|}{\Delta x\left(1+\frac{D_{\rho_i}}{\rho_i}\frac{\Delta x}{6}\right)}, \frac{1}{\Delta t}\right) \tag{41}$$

For the Euler system, a limiter with a constraint to ensure the positivity of the energy is applied to the velocities:

$$D_{u_i,Euler} = \frac{1}{2}\left(\text{sign}(u_{i+1}-u_i)+\text{sign}(u_i-u_{i-1})\right)\min\left(\frac{|u_{i+1}-u_i|}{\Delta x\left(1-\frac{D_{\rho_i}}{\rho_i}\frac{\Delta x}{6}\right)}, \frac{|u_i-u_{i-1}|}{\Delta x\left(1+\frac{D_{\rho_i}}{\rho_i}\frac{\Delta x}{6}\right)}, D_{u_i}^{\max,\sigma_i}, \frac{1}{\Delta t}\right) \tag{42}$$

where:

$$D_{u_i}^{\max,\sigma_i} = \sqrt{\frac{\sigma_i}{\frac{\Delta x^2}{12}\left(1+\frac{\Delta x^2}{12}\frac{D_{\rho_i}^2}{\rho_i^2}\right)}} \tag{43}$$

Finally, for the Euler system a similar slope limitation is applied to the variance:

$$D_{\sigma_i} = \frac{1}{2}\left(\text{sign}(\sigma_{i+1}-\sigma_i)+\text{sign}(\sigma_i-\sigma_{i-1})\right)\min\left(\frac{|\sigma_{i+1}-\sigma_i|}{\Delta x\left(1-\frac{D_{\rho_i}}{\rho_i}\frac{\Delta x}{6}\right)}, \frac{|\sigma_i-\sigma_{i-1}|}{\Delta x\left(1+\frac{D_{\rho_i}}{\rho_i}\frac{\Delta x}{6}\right)}\right) \tag{44}$$

The extension of this method to the AG model is developed and evaluated in the work of Vié et al. [3].

3.2.3 Fluxes Evaluation

Following the reconstruction an approximate Riemann solver is used for the fluxes evaluation, for which the right and left states at the interface results from the reconstruction procedure. For the scheme in question, an HLL approximate Riemann solver is chosen [43].
For example, if we take the advection equation of the moments in one direction:

$$\partial_t \mathbf{M} + \partial_x \mathcal{F}(\mathbf{M}) = 0 \tag{45}$$

Given the initial states of each side of the interface $\mathbf{M}_L$ and $\mathbf{M}_R$ with fluxes $\mathcal{F}(\mathbf{M}_L)$ and $\mathcal{F}(\mathbf{M}_R)$ respectively, the intermediate state is found by integrating eqn (45):

$$\mathbf{M}^* = \frac{\mathbf{M}_L-\mathbf{M}_R}{\lambda_{min}-\lambda_{max}} - \frac{\mathcal{F}(\mathbf{M}_L)-\mathcal{F}(\mathbf{M}_R)}{\lambda_{min}-\lambda_{max}} \tag{46}$$

where R and L stand respectively for the right and left side of the interface; and λ_{max} and λ_{min} are respectively the maximum and minimum eigenvalues of the Jacobian of the fluxes at the interface. Then, the fluxes at the interface are:

$$\mathcal{F}^{HLL}(\mathbf{M}_L,\mathbf{M}_R) = \frac{1}{2}\left(\mathcal{F}(\mathbf{M}_L)+\mathcal{F}(\mathbf{M}_R)\right) - \frac{1}{2}|\lambda_{min}|\left(\mathbf{M}^*-\mathbf{M}_L\right) - \frac{1}{2}|\lambda_{max}|\left(\mathbf{M}_R-\mathbf{M}^*\right) \tag{47}$$

Finally, using a 2-step Runge-Kutta method for the integration in time, one gets:

$$\begin{aligned}\mathbf{M}_i^{n+1/2} &= \mathbf{M}_i^n - \frac{1}{2}\frac{\Delta t}{\Delta x}\left(\mathcal{F}_{i+1/2}^n - \mathcal{F}_{i-1/2}^n\right)\\ \mathbf{M}_i^{n+1} &= \mathbf{M}_i^n - \frac{\Delta t}{\Delta x}\left(\mathcal{F}_{i+1/2}^{n+1/2} - \mathcal{F}_{i-1/2}^{n+1/2}\right)\end{aligned} \tag{48}$$

In fact, the 2-step Runge-Kutta method can be perfomed in another way in order to have a SSP time integrator, in the current work we choose the first method since it is less memory consuming [24]. The resulting scheme is a second order scheme in time and space which preserves the realizablity of the moments. It is an accurate, stable and realizable scheme on structured meshes.

4. 2D RESULTS AND DISCUSSIONS

4.1 Test Cases: Homogenous Isotropic Turbulence

In order to assess the DG method, a two-dimensional test case is investigated. It represents a one-way interaction between a periodic 3x3 frozen homogenous isotropic turbulent velocity field (HIT) and a spray which is homogeneous at $t = 0$. The HIT has been generated with the ASPHODELE code of CORIA, which solves the three-dimensional Navier-Stokes equations for the gas phase under the low-Mach assumption [44]. The properties of this HIT are shown in Table 1, where Re_t is the turbulent Reynolds number, u_t is the velocity root-mean-square, ε is the mean dissipation rate, η_K is the smallest structures scale, l_{int} is the integral scale of the turbulence, τ_K is the Kolmogorov time scale of the turbulence, and τ_{int} is the eddy turnover time.

Table 1. Turbulence properties of the HIT

Re_t	u_t	ε	η_K	l_{int}	τ_K	τ_{int}
7.12	0.1	0.01	0.022	0.1	0.36	1.0

This fundamental test case is chosen not only to conduct a general comparison between the results of different schemes, but also to be able to examine the segregation and to assess the diffusivity and robustness of the numerical methods.

The study is conducted for the two models presented in the second section, i.e. the monokinetic and the isotropic Gaussian closure, for two different Stokes numbers with respect to the Kolmogorov time scale of the turbulence, namely 0.8 and 4.2. For the sake of comparison and in order to have a physical reference, a Lagrangian Discrete Particle Simulation is done for each of these Stokes number. Ten million particles are used, ensuring a satisfactory statistical convergence. The Lagrangian results for the number density are computed after a time large enough with respect to the relaxation time of the particles τ_p in order to catch the real dynamic of the flow including any possible high concentration regions and vacuum zones (see Figure 5). At small Stokes number (St=0.8), strong segregation effects occur: particles are gathered in low vorticity zones, and no or negligible PTC is encountered, so that the two considered models should provide suitable results. On the other hand, at a higher Stokes number St=4.2, particles with greater inertia do not accumulate in the low vorticity zones. They start oscillating around equilibrium trajectories and generate PTC. In this context, the MK model will fail to predict this type of dynamics; therefore we only investigate the Isotropic Gaussian model for this Stokes number. In order to compare the number density of the particles obtained by the two methods at a given time, we consider a 128^2 quadrangular mesh for the FV and the same mesh for DG where quadrangles have been cut into triangles (so if we refer to a 128^2-cell mesh for the DG results it means that we have trianglular mesh based on the 128^2 quadrangular mesh). Computation is performed for the two models at St=0.8 and a snapshot is taken after a time long enough ($4\tau_{int}$). The same thing is repeated at St=4.2 for the Isotropic Gaussian closure models. Finally, the segregation of particles G^{Δ}_{pp} is investigated, which corresponds to the spatial correlation of the number density field at a given cell size length [21]:

$$G^{\Delta}_{pp} = \frac{\langle \rho(x)\rho(x+\Delta x)\rangle}{\langle \rho(x)\rangle^2} = \frac{\langle \rho^2\rangle}{\langle \rho\rangle^2} \tag{49}$$

where $\langle . \rangle$ is the averaging operator over the whole domain. And, for the sake of comparison, the segregation is always calculated on a 64^2 quadrangular mesh, the result of the finer meshes being projected on this reference mesh.

The evolution of the segregation with time is analyzed. It quantifies the degree of accumulation of droplets in the high concentration region, as well as the degree of depletion in the vacuum zones. Three different meshes are considered namely 64^2, 128^2 and 256^2 for both models and both numerical schemes. These results are compared with one another, but also with two references, namely the statistically converged Lagrangian simulation and a highly refined finite volume solution on a

1024^2-cell mesh. The Lagrangian result is the physical reference as it contains all the physics. The FV segregation on the 1024^2-cell mesh is the numerical reference, because it should encounter a significantly lower numerical diffusion, thus being closer to the solution of the considered model at mesh convergence.

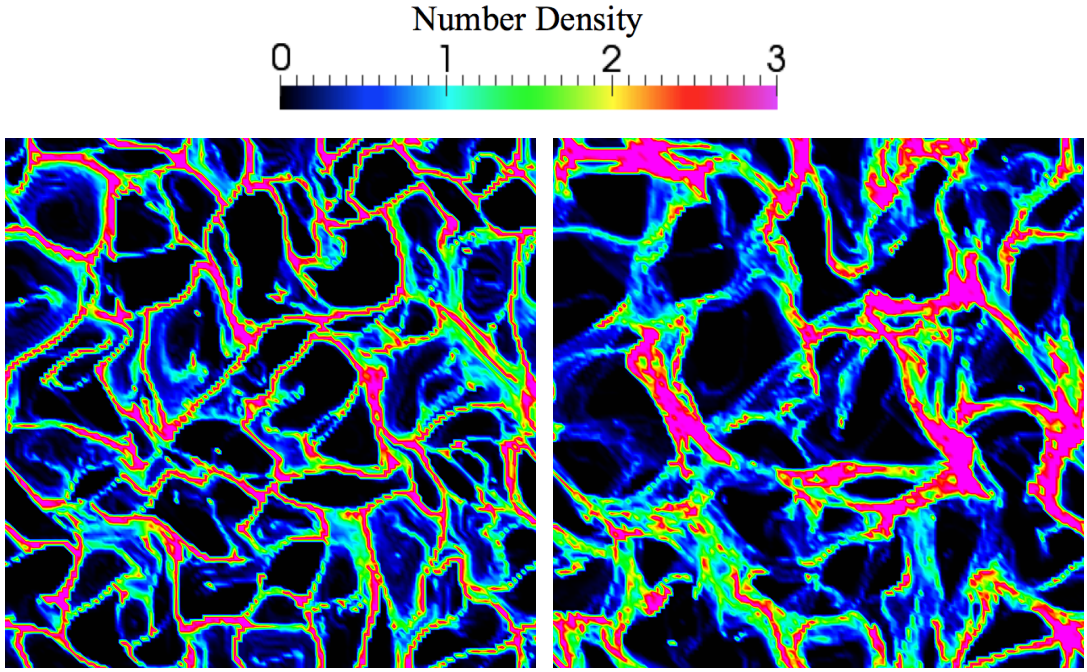

(a) Lagrangian results for St=0.8 at t=4 (b) Lagrangian results for St=4.2 at t=12

Figure 5. Snapshots of the particles number density solved by the Lagrangian approach

4.2 First Test Case: Monokinetic-HIT

In Figure 6, the results of the MK model is shown for St=0.8. The structure in these figures matches qualitatively the Lagrangian result given in Figure 5. This is expected since for the low inertia particles we do not have considerable PTC. However, due to numerical diffusion, the solution is smeared out. This diffusivity affects particularly the solution of the FV scheme as seen in Figure 6(a). The fact that the DG method provides finer structures and more droplet clusters than the FV for the same mesh is pointed out here and is quantified through the segregation study, see Figure 7 and its analysis in the next paragraph. This case illustrates the low numerical diffusivity of the second order DG method compared to the FV one.

In Figure 7, we show the evolution with time of the segregation, for different meshes and for a particle Stokes number equal to 0.8. For a given mesh, the segregation of the DG results is higher than the one of the FV solutions and it is also closer to the Lagrangian segregation. The segregation rate of the DG solution for a given mesh (N^2) is quantitatively comparable to the one of the FV solution for a mesh which is at least twice as refined as the mesh used for the DG solution $(2N)^2$. Now, if we compare the segregation of the DG solution for a refined mesh (256^2) with the one of the highly refined FV solution (1024^2), we note that the curve of the segregation of the DG solution is slightly beneath the refined FV segregation curve. Also, the segregations for the two numerical schemes tend to be asymptotic with the Lagrangian profile when refining the mesh. This proves two points:

- the MK model has the ability to reproduce the high segregation effects
- the DG method is found to be less diffusive than the FV one.

In reality, a more accurate finite volume scheme for this model is found in the literature [26, 29]. It is the finite volume kinetic scheme (FVKS) for pressureless gas dynamics system. In this article, we compare the DG results to the MUSCL/HLL results only since this latter (unlike the FVKS) is

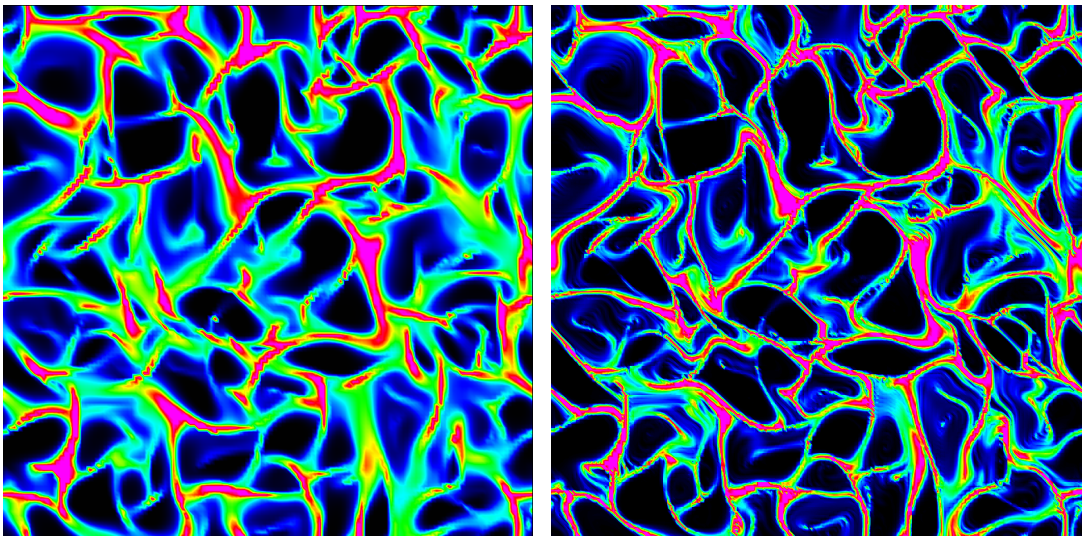

(a) Reference solution with a 2^{nd} order FV (b) 2^{nd} order DG solution

Figure 6. Particles number density at t=4 for the problem with MK closure for a Stokes number of 0.8 and a 128^2-cell mesh

suitable for solving both the PGD and Euler systems. In future work, further comparison will be carried out between the results of the FVKS and the DG results in the case of MK closure.

From a computational cost point of view, for a given mesh the FV method is cheaper than the DG method but it will give results of lower quality. The additional cost for DG method is caused mainly by the integration by quadrature and the realizability preservation. For the FV scheme we have four degrees of freedom per cell. This quadrangle is divided into two triangles in the case of DG [2] having 3 DOFs each. So, for the same mesh DG has 1.5 times more DOFs and should be therefore more precise. For a given mesh, the ratio of time per DOF is nearly 10 times higher for the DG scheme. In order to assess the cost to quality ratio, one needs to compare the cost of the two methods for the

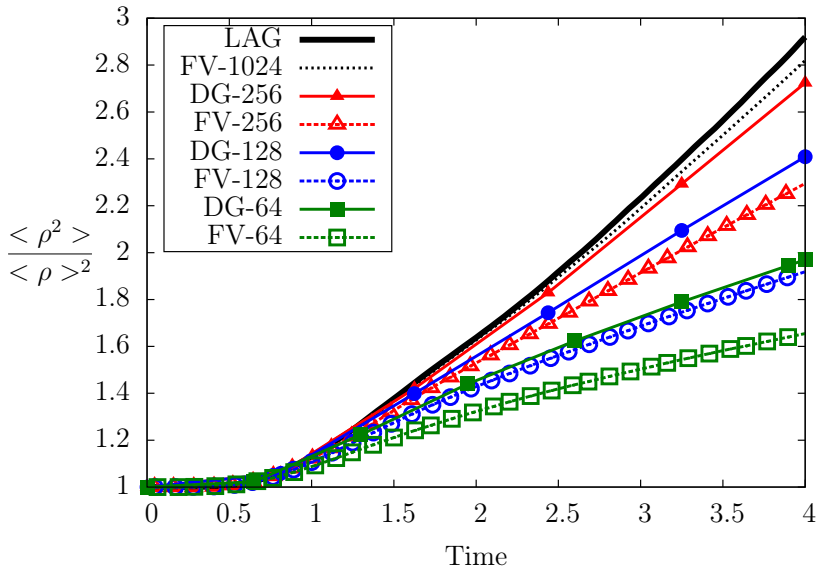

Figure 7. Evolution of the segregation with time for the Lagrangian and MK model using FV and DG method with different meshes for a Stokes number of 0.8

[2]It is important to note that a study on totally unstructured mesh with DG in 2-D was already done but will not be presented here; for more information one may refer to the CTR Annual Research Brief of Larat et al. [5].

same result accuracy. The DG solutions with 64^2 and 128^2-cell meshes are comparable to the FV results with 128^2 and 256^2-cell meshes respectively. In this case the DG results is two times more expensive than the FV results. On the other hand, if one consider the numerical solution given by the DG approach for 256^2-cell mesh which is qualitatively (see Figure 8) and quantitatively comparable to the FV result for the 1024^2-cell mesh, DG is found to be more than four times faster in this case. In fact, the segregation study with DG (refined mesh, 256^2) took around 52 minutes while nearly 4 hours of computation were spent for an equivalent result with FV (highly refined mesh 1024^2 cells) knowing that the degrees of freedom (DOF) in this case are greater for FV see Table 2.

Table 2. CPU computation time in seconds and Degree Of Freedom for different meshes for DG and FV results with MK closure for a Stokes number of 0.8

Mesh	**64^2**	**128^2**	**256^2**	**1024^2**
Time DG	43.05	384.04	3130.05	–
Time FV	2.84	24.45	180.02	13583.41
DOF DG	24576	98304	393216	6291456
DOF FV	16384	65536	262144	4194304
Time/DOF DG	0.00175	0.00391	0.00796	–
Time/DOF FV	0.00017	0.00037	0.00069	0.00324

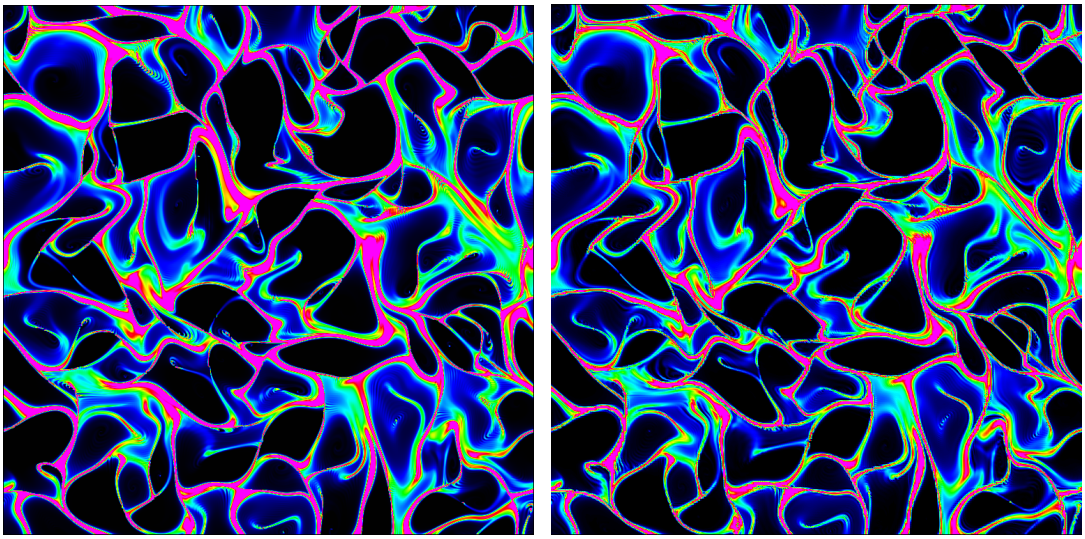

(a) Reference solution with a 2^{nd} order FV with a 1024^2-cell mesh

(b) 2^{nd} order DG solution with a 256^2cell mesh

Figure 8. Particles number density at t=4 for the problem with MK closure for a Stokes number of 0.8 with a 1024^2-cell mesh for the FV results and a 256^2-cell mesh for the DG results

4.3 Second Test Case: Isotropic Gaussian- HIT

In Figures 9 and 10 the results of the isotropic Gaussian model are shown respectively for St=0.8 and St=4.2.
At St=0.8, the model reproduces the general Lagrangian structure but the result is more spread out than the one given by the Lagrangian method or by the MK model using DG. Some of the fine highly concentrated clusters are widened, and the stiff regions in the FV result are clearly more diffused than those of the DG solution.

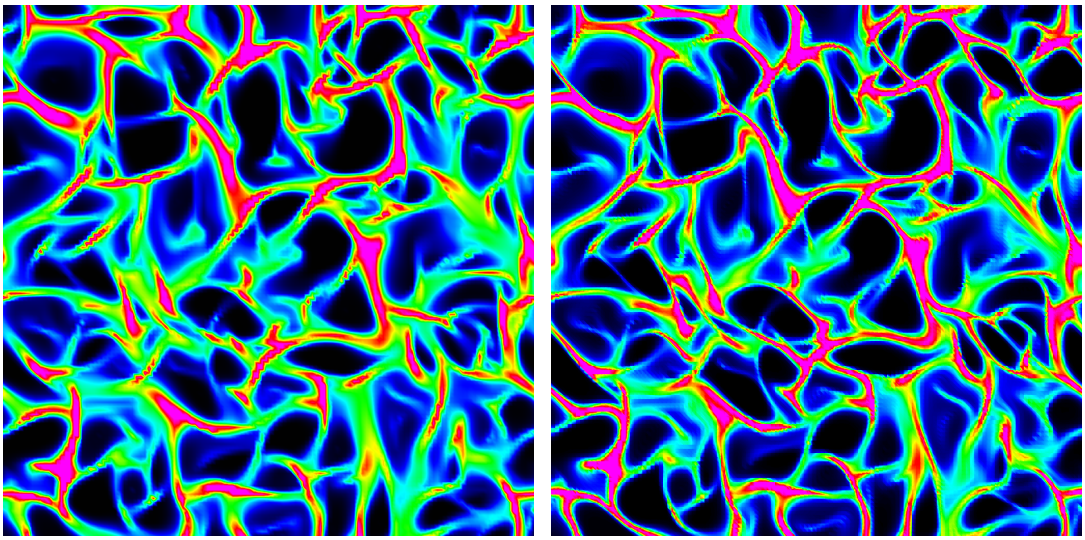

(a) Reference solution with a 2^{nd} order FV (b) 2^{nd} order DG solution

Figure 9. Particles number density at t=4 for the HIT problem with isotropic Gaussian closure for a Stokes number equal to 0.8 and a 128^2-cell mesh

At St=4.2, the isotropic Gaussian closure model captures the global structures of the Lagrangian reference solution. However, on the contrary to the results at lower Stokes number, it shows some finer ligaments than the Lagrangian solution.

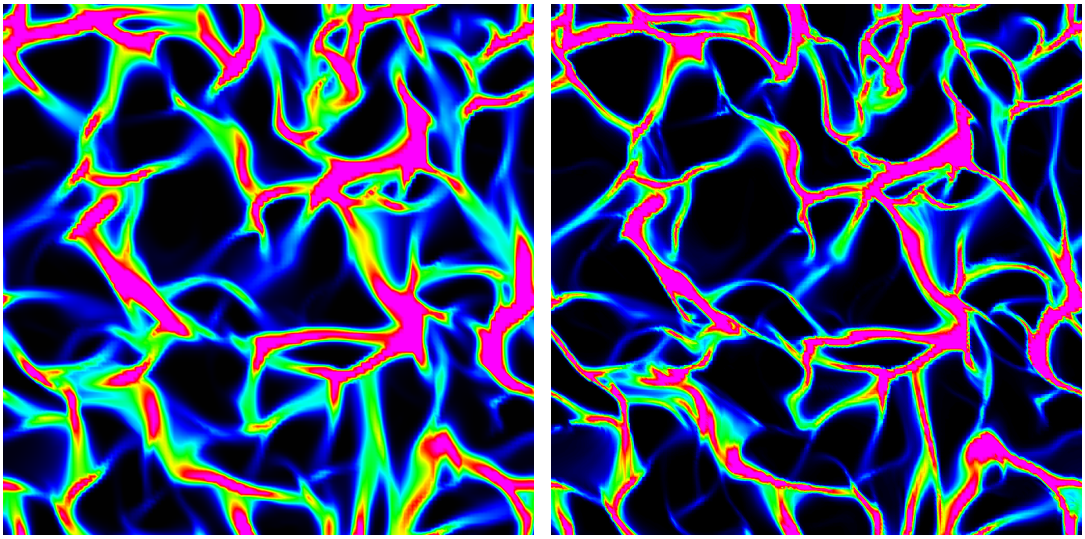

(a) Reference solution with a 2^{nd} order FV (b) 2^{nd} order DG solution

Figure 10. Particles number density at t=12 for the HIT problem with isotropic Gaussian closure for a Stokes number equal to 4.2 and a 128^2-cell mesh

In fact, by comparing the numerical results to the Lagrangian one, the effect of the model on the results is observed. The model in question is limited by the isotropic assumption [3], so the preferential accumulations are overestimated using this model compared to the Lagrangian result. In addition, by comparing the numerical results for a given model, the effect of numerical diffusion[3] will be pointed out. Qualitative observations of the snapshot of Figure 9 and Figure 10, once more show a lower numerical diffusion by the DG approach compared to the FV technique.
The latter conclusion needing to be quantitatively assessed, the evolution of the segregation with time

[3]The numerical diffusion spreads out the structures, and lowers the segregation.

for different meshes, for two Stokes numbers St=0.8 and St=4.2 is shown respectively in Figures 11 and 12.

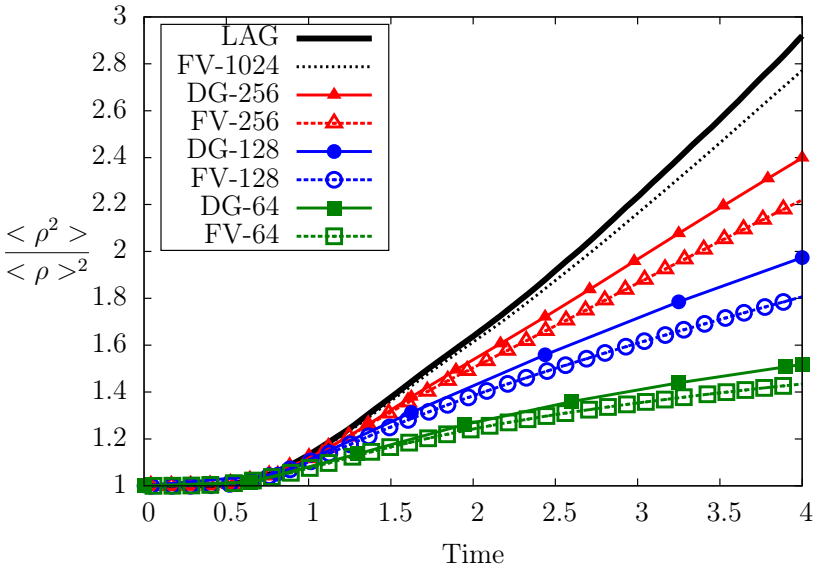

Figure 11. Evolution of the segregation with time for the Lagrangian and isotropic Gaussian closure model using FV and DG method with different meshes for a Stokes number of 0.8

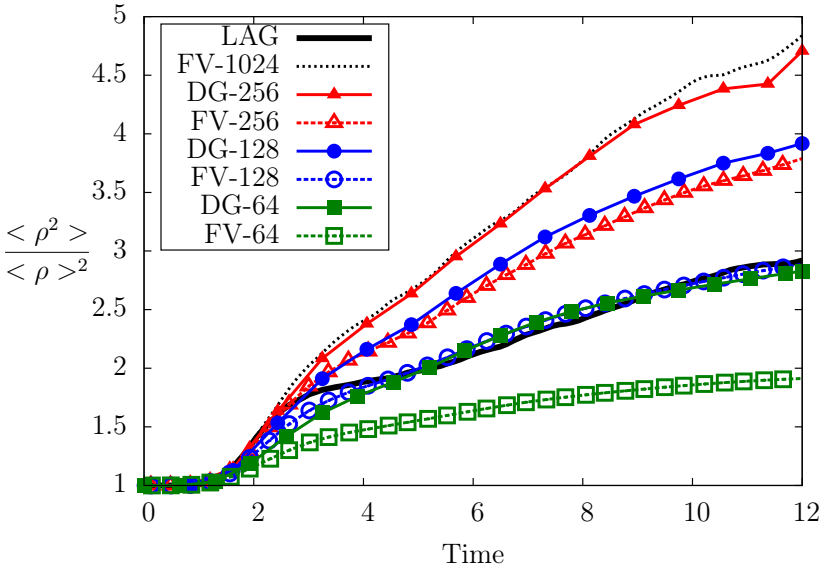

Figure 12. Evolution of the segregation with time for the Lagrangian and isotropic Gaussian closure model using FV and DG method with different meshes for a Stokes number of 4.2

For low inertia particles, the segregation profiles for the two schemes tends to converge to the Lagrangian one when the mesh is refined but for the same mesh the MK model provides a steeper profile than the isotropic Gaussian model. For a given mesh, the segregation of the DG results is higher than the segregation of the FV solutions. In the case of moderate Stokes number, the segregation profile for this model is diverging from that of the Lagrangian; the model is no more capturing the physics of the flow. The difference between temporal evolution of segregation of the Lagrangian method and the numerical methods is due to the inappropriateness of the model as detailed by Vié et al. [3]. From a numerical point of view, the segregation using DG for the refined

mesh (256^2) is nearly equivalent to the one of FV with a 1024^2-cell mesh. And in general the segregation using DG is higher than the segregation using FV for the same mesh. Here DG also has a level of convergence significantly higher than FV. From a modeling point of view, this model was found to be unsuitable for describing the physics of moderately inertial particles because of the unphysical high segregation. In fact, the PTC are intrisically anisotropic so that the isotropic model is too restrictive and therefore it overestimates the segregation since it underestimates the mean central energy [3].

4.4 Towards Predictive Simulations: Anisotropic Gaussian- HIT

The Gaussian closure is the first class of pressure-like models for capturing PTC. However, the isotropic assumption is too restrictive to reproduce crossings induced by the shear zones, which are intrinsically anisotropic [3]. Therefore, the next step of our study is to adapt the DG approach to the AG closure. To highlight the potential of such a modeling approach, we compare the results at St=4.2 for the isotropic and Anisotropic Gaussian closure with the FV scheme. The MUSCL/HLL scheme used for the AG model is developed by Vié et al. [3].
For the segregation study we take three meshes, namely a 64^2-cell mesh and a 128^2-cell mesh and a 256^2-cell mesh. On the one hand, the Isotropic closure results shown in Figure 10(a) differ significantly from the Lagrangian results (Figure 13(b)). Even if it actually captures the global structure of the solution, it clearly overestimates the preferential accumulation effects. On the other hand, the Anisotropic closure results (Figure 13(a)) using the same mesh (i.e. 128^2) quanlitatively match the Lagrangian results with a slight underestimation of the preferential accumulation effects.

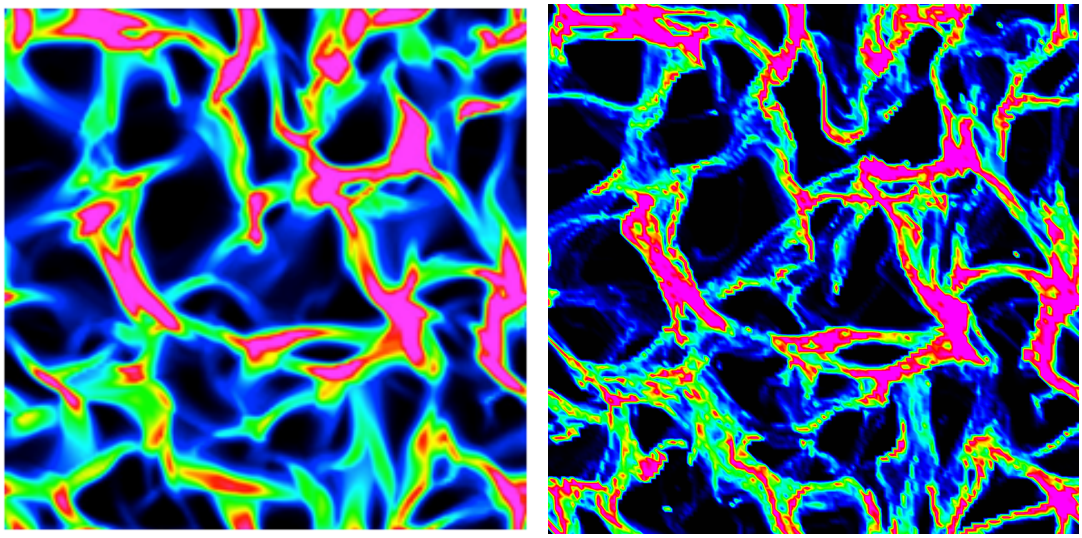

(a) Anisotropic Gaussian model using the 2nd order FV scheme for a 128^2-cell mesh, St=4.2 at t=12

(b) Lagrangian results for St=4.2 at t=12

Figure 13. Particles number density at t=12 for the HIT problem with the Anisotropic Gaussian model using 2nd order FV scheme and the Lagrangian solution for a Stokes number equal to 4.2

In addition, the comparison of the segregations, in Figure 14, demonstrates that the AG closure does not create unphysical accumulations, as the segregation is still below the Lagrangian segregation, where the isotropic Gaussian closure leads to highly overestimated segregation for a moderate refinement.

Finally, the segregation trend of the Anisotropic closure result tends to converge to the Lagrangian one so that whenever the mesh is refined the profile will stay below the Lagragian profile, whereas the Isotropic segregation curves diverges already for relatively coarse meshes. It is thus clear that more realistic simulations must rely on this new closure since it can account for the anisotropic behavior in the case of PTC.

For a more detailed comparison between the isotropic and AG results on 2D Taylor-Green vortices and time-evolving HIT test cases, one may refer to the work of Vié et al. [3].

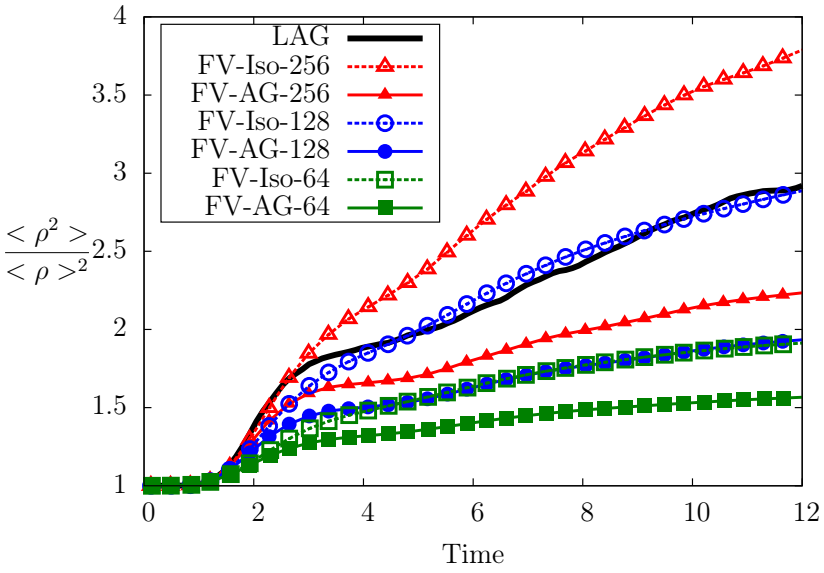

Figure 14. Evolution of the segregation with time for the Lagrangian, isotropic Gaussian closure, and Anisotropic Gaussian closure model using FV for a Stokes number of 4.2

5. CONCLUSION

When it comes to numerical methods, the proposed realizable DG scheme has proven to be robust and accurate. This scheme respects the realizability conditions and can be used on unstructured meshes, which are crucial for real complex geometries. It is less diffusive in comparison with the various second order FV scheme, and for the studied cases more competitive. For the sake of comparison, an algorithmic complexity analysis should be carried out for the two schemes.

From a modeling point of view, the MK closure is suitable for low Stokes number. Besides, for moderate Stokes number the Isotropic Gaussian closure model is not reproducing the physics of the problem accurately. Other Eulerian modeling methods of higher order in moments and higher level in the hierarchy of models have to be therefore used. A first model is the Anisotropic Gaussian closure model and is shown to reproduce the physics of particle trajectory crossing for a relatively large range of Stokes number.

Therefore, further work should be done to relate the proposed realizable DG scheme to higher order models starting with the AG model; it is a work in progress. Further comparisons between the DG and the MUSCL/HLL results should be carried out for this model. In addition, an indispensable comparison between the DG scheme and the finite volume kinetic scheme for the MK closure model is also envisaged in future work.

One of the perspectives is also to extend this work to higher orders DG schemes and to three-dimensional space. The extension to three-dimensional space of the comparison DG-FV is essential since the DG scheme is known to be quite computationally expensive: it is one of the reasons that makes it mostly unused in industrial codes. This highlights the importance of a cost/quality comparison (similar to the one presented in this work) between the 3-D results of the DG and the MUSCL/HLL schemes.

ACKNOWLEDGMENTS

The support of SNECMA for this research is gratefully acknowledged. Part of the results presented in this work were obtained during the CTR Summer Program 2012, hence the authors would like to thank the CTR for their technical and financial support of Adam Larat stay and the SAFRAN group for the stay of Aymeric Vié.
The France-Stanford Center for Interdisciplinary Studies is also gratefully acknowledged for their support through the collaborative project grant (P. Moin / M. Massot).

References

[1] F. Laurent and M. Massot. Multi-fluid modeling of laminar poly-dispersed spray flames: origin, assumptions and comparison of the sectional and sampling methods. *Combustion Theory and Modelling*, 5: 537–572, 2001.

[2] M. Massot. *Eulerian multi-fluid models for polydisperse evaporating sprays*, volume 492 of *CISM Courses and Lectures*, chapter in "Multiphase Reacting Flows: Modelling and Simulation", *Udine, July 2006*, pages 79–123. Springer Wien New York (2007), 2007. D.L. Marchisio and R.O. Fox Editors.

[3] A. Vié, F. Doisneau, and M. Massot. On the Anisotropic Gaussian closure for the prediction of inertial-particle laden flows. *Submitted to Communications in Computational Physics*, 2013. Available on HAL : http://hal.archives-ouvertes.fr/hal-00912319.

[4] S. de Chaisemartin, L. Fréret, D. Kah, F. Laurent, R. Fox, J. Reveillon, and M. Massot. Eulerian models for turbulent spray combustion with polydispersity and droplet crossing. *Comptes Rendus Mécanique*, 337:438–448, 2009. Special Issue 'Combustion for Aerospace Propulsion'.

[5] A. Larat, M. Massot, and A. Vié. A stable, robust and high order accurate numerical method for eulerian simulation of spray and particle transport on unstructured meshes. In *Annual Research Briefs 2012*, pages 205–216, Center for Turbulence Research, Stanford University, USA, 2012.

[6] X. Zhang, Y. Xia, and C.-W. Shu. Maximum-principle-satisfying and positivity-preserving high order discontinuous galerkin schemes for conservation laws on triangular meshes. *Journal of Scientific Computing*, 50(1):29–62, 2012.

[7] X. Zhang and C.-W. Shu. On maximum-principle-satisfying high order schemes for scalar conservation laws. *Journal of Computational Physics*, 229(9):3091–3120, 2010.

[8] X. Zhang. *Maximum-Principle-Satisfying and Positivity-Preserving High Order Schemes for Conservation Laws*. PhD thesis, Brown University, 2011.

[9] B. Van Leer. Towards the ultimate conservative difference scheme V. A second order sequel to Godunov's method. *Journal of Computational Physics*, 32(1):101–136, 1979.

[10] V. le Chenadec and H. Pitsch. A monotonicity preserving conservative sharp interface flow solver for high density ratio two-phase flows. *Journal of Computational Physics*, 249:185–203, 2013.

[11] F. Williams. Spray combustion and atomization. *Physics of Fluids*, 1:541–545, 1958.

[12] J. Dukowicz. A particle-fluid numerical model for liquid sprays. *Journal of Computational Physics*, 35 (2):229–253, 1980.

[13] P. J. O'Rourke. *Collective drop effects on vaporizing liquid sprays*. PhD thesis, Princeton University, 1981.

[14] S. Subramaniam. Lagrangian-eulerian methods for multiphase flows. *Progress in Energy and Combustion Science*, 231(2-3):215–245, 2013.

[15] J. P. Minier and E. Peirano. The pdf approach to polydispersed turbulent two phase flows. *Physics Reports*, 352(1-3):1–214, 2001.

[16] S. Chibbaro and J. P. Minier. A note on the consistency of hybrid Eulerian/Lagrangian approach to multiphase flows. *International Journal of Multiphase Flow*, 37(3):293–297, 2011.

[17] M. Garcia. *Development and validation of the Euler-Lagrange formulation on a parallel and unstructured solver for large-eddy simulation*. PhD thesis, Université Toulouse III, 2009. available online at http://ethesis.inp-toulouse.fr/archive/00000715/.

[18] A. Kaufmann, M. Moreau, O. Simonin, and J. Helie. Comparison between Lagrangian and mesoscopic Eulerian modelling approaches for inertial particles suspended in decaying isotropic turbulence. *Journal of Computational Physics*, 227:6448–6472, 2008.

[19] E. Masi and O. Simonin. An algebraic-closure-based moment method for unsteady Eulerian modeling of non-isothermal particle-laden turbulent flows in very dilute regime and high Stokes number. *Turbulence, Heat and Mass Transfer*, 7:1–12, 2012.

[20] C. Chalons, D. Kah, and M. Massot. Beyond pressureless gas dynamics: quadrature-based velocity moment models. *Communication in Mathematical Sciences*, 10(4):1241–1272, 2012.

[21] O. Simonin, L. Zaichik, V. Alipchenkov, and P. Février. Connection between two statistical approaches for the modelling of particle velocity and concentration distributions in turbulent flow: The mesoscopic eulerian formalism and the two-point probability density function method. *Physics of Fluids*, 18(12): 125107(1–9), 2006.

[22] G. Dufour, M. Massot, and P. Villedieu. Étude d'un modèle de fragmentation secondaire pour les brouillards de gouttelettes. *C. R. Math. Acad. Sci. Paris*, 336(5):447–452, 2003.

[23] C. Yuan and R. Fox. Conditional quadrature method of moments for kinetic equations. *Journal of Computational Physics*, 230(22):8216–8246, 2011.

[24] A. Vié, F. Laurent, and M. Massot. Size-velocity correlations in hybrid high order moment/multi-fluid methods for polydisperse evaporating sprays: modeling and numerical issues. *Journal of Computational Physics*, 237:177–210, 2013.

[25] J. Dombard. *Direct Numerical Simulation of non-isothermal dilute sprays using the Mesoscopic Eulerian Formalism*. PhD thesis, INP Toulouse, 2011.

[26] F. Bouchut, S. Jin, and X. Li. Numerical approximations of pressureless and isothermal gas dynamics. *SIAM Journal on Numerical Analysis*, 41:135–158, 2003.

[27] D. Kah, F. Laurent, M. Massot, and S. Jay. A high order moment method simulating evaporation and advection of a polydisperse spray. *Journal of Computational Physics*, 231(2):394–422, 2012.

[28] O. Colin and M. Rudgyard. Development of high-order Taylor-Galerkin schemes for LES. *Journal of Computational Physics*, 162(2):338–371, 2000.

[29] S. de Chaisemartin. *Eulerian models and numerical simulation of turbulent dispersion for polydisperse evaporation sprays*. PhD thesis, Ecole Centrale Paris, France, 2009. Available on TEL : http://tel.archives-ouvertes.fr/tel-00443982/en/.

[30] F. Laurent, M. Massot, and P. Villedieu. Eulerian multi-fluid modeling for the numerical simulation of coalescence in polydisperse dense liquid sprays. *Journal of Computational Physics*, 194:505–543, 2004.

[31] F. Doisneau, F. Laurent, A. Murrone, J. Dupays, and M. Massot. Eulerian multi-fluid models for the simulation of dynamics and coalescence of particles in solid propellant combustion. *Journal of Computational Physics*, 234:230–262, 2013.

[32] C. Levermore and W. Morokoff. The Gaussian moment closure for gas dynamics. *SIAM Journal on Applied Mathematics*, 59(1):72–96, 1998.

[33] C. Chalons, R. Fox, F. Laurent, M. Massot, and A. Vié. A multi-Gaussian quadrature- based moment method for dispersed multiphase flows. *Submitted to SIAM Journal on Multiscale Modeling and Simulation*, 2013.

[34] L. Fréret, O. Thomine, F. Laurent, J. Reveillon, and M. Massot. On the ability of the eulerian multi-fluid model to predict preferential segregation and flame dynamics in polydisperse evaporating sprays. *Submitted to Combustion and Flame*, 2013.

[35] F. Bouchut. On zero pressure gas dynamics. In *Advances in kinetic theory and computing*, volume 22 of *Ser. Adv. Math. Appl. Sci.*, pages 171–190. World Sci. Publ., River Edge, NJ, 1994.

[36] Y. Brenier and E. Grenier. Sticky particles and scalar conservation laws. *SIAM Journal of Numerical Analysis*, 35:2317–2328, 1998.

[37] H. Dette and W. J. Studden. *The theory of canonical moments with applications in statistics, probability, and analysis*. Wiley Series in Probability and Statistics. John Wiley & Sons Inc., New York, 1997.

[38] R. J. LeVeque. *Finite volume methods for hyperbolic problems*. Cambridge Texts in Applied Mathematics. Cambridge University Press, Cambridge, 2002.

[39] X. Zhang and C.-W. Shu. Positivity-preserving high order discontinuous galerkin schemes for compressible euler equations with source terms. *J. Comput. Phys.*, 230(4):1238–1248, Feb. 2011.

[40] B. Cockburn and C.-W. Shu. The Runge-Kutta discontinuous Galerkin method for conservation laws V - multidimensional systems. *Journal of Computational Physics*, 141(2):199–124, 1998.

[41] S. Gottlieb, D. I. Ketcheson, and C.-W. Shu. High order strong stability preserving time discretizations. *J. Sci. Comput.*, 38(3):251–289, 2009.

[42] C. Berthon. Stability of the MUSCL schemes for the euler equations. *Communications in Mathematical Sciences*, 3(2):133–157, 2005.

[43] A. Harten, P. D. Lax, and B. van Leer. On upstream differencing and Godunov-type schemes for hyperbolic conservation laws. *SIAM Review*, 25(1):35–61, 1983.

[44] L. Guichard, J. Reveillon, and R. Hauguel. Direct numerical simulation of statistically stationary one- and two- phase turbulence combustion: a turbulent injection procedure. *Flow, Turbulence and Combustion*, 73:133–167, 2004.